State-Resolved Photofragment Velocity Distributions by Pulsed Extraction Time-of-Flight Mass Spectrometry

R. Ogorzalek Loo, G. E. Hall, H.-P. Haerri, and P. L. Houston*

Department of Chemistry, Cornell University, Ithaca, New York 14853 *(Received: October 9, 1987; In Final Form: November 16, 1987)*

Two new methods for simultaneous measurement of velocity and internal state are reported, and results are presented for application of the techniques to the photodissociation of CH_3I. The internal state of the probed fragment is chosen by tuning the resonant ionizing laser, while the fragment velocity is determined from the arrival time distribution of fragment ions at the detector of a time-of-flight (TOF) mass spectrometer. For the 266-nm dissociation of CH_3I or CD_3I, the amount of $I^*(^2P_{1/2})$ vs $I(^2P_{3/2})$ produced in coincidence with $CH_3(\nu_2=i)$ or $CD_3(\nu_2=j)$ has been determined for $i = 0$–2 and $j = 0$–3. The values are $(i, I/I^*) = (0, 0.08), (1, 0.37), (2, 1.1)$ and $(j, I/I^*) = (0, <0.05), (1, 0.09), (2, 0.19), (3, 0.68)$. These I/I^* ratios were found to vary dramatically with probe wavelength, partly due to variations in ratio with methyl rotational level and partly due to different contributions from overlapping vibronic bands. In a further application, separate MPI wavelength scans were obtained simultaneously for CD_3 produced in coincidence with I and I*. Observations on the I and I* fragments have allowed us to determine values for the anisotropy parameters ($\beta(I) = 1.7 \pm 0.1$, $\beta(I^*) = 1.8 \pm 0.1$). Application of these techniques to the detection of clusters and to the discrimination between multiple pathways to the same fragment ion in multiphoton dissociation and ionization is discussed.

Introduction

Many problems in molecular dynamics, including molecular photodissociation, require the simultaneous measurement of velocity and internal energy. Early photofragment spectrometers were designed to measure either the recoil velocity distribution[1,2] or the internal energy of the fragments,[3,4] but it has only been recently that correlated measurements of these properties have been obtained. A Doppler technique has been developed to obtain the projection of the velocity distribution onto the detection direction.[5] Early applications have investigated the photodissociations of HI[6] and ICN;[7] a subsequent modification uses the Doppler technique to determine kinetic energy distributions.[8,9] A time-of-flight (TOF) technique for measuring a projection of the velocity distribution for state-selected photofragments has been briefly described in a previous publication;[10] further details and results are presented in this Letter. More recently, an imaging technique has been reported in which the velocity distribution for state-selected fragments is projected onto a two-dimensional detector.[11]

In this Letter we describe two variations on the TOF technique. Either a one-dimensional projection of the velocity distribution or a one-dimensional sample through the core of the full three-dimensional distribution is obtained by the unconventional use of a standard TOF mass spectrometer. The one-dimensional projection technique, as previously described,[10] is fully equivalent to the Doppler method but requires neither sub-Doppler laser line widths nor uncongested spectra. Our methods are applied here to the photodissociation of CH_3I, whose photophysics have been discussed in detail elsewhere.[12-16]

Experimental Section

The experimental apparatus, similar in design to systems described previously,[17] employs a pulsed supersonic nozzle source, two skimmers, and a Wiley-McClaren time-of-flight mass spectrometer.[18] Extraction and acceleration voltages, V_{ex} and V_{acc}, are generated by a Velonex Model 350 high-voltage pulsed power supply with a measured risetime of about 50 ns (2 kV into 200 Ω). The focused photolysis (quadrupled Nd:YAG) and focused probe laser (doubled Nd:YAG-pumped dye laser) intersect each other and the molecular beam at a location 8 mm upstream from the vertical center line of the mass spectrometer and are timed so that fragment ionization follows the parent photolysis by 25 ns. Field-free conditions are maintained for a time (τ_d) during which the photoions recoil with the velocity imparted to them by the neutral dissociation. After this delay, the ions are extracted and accelerated up the flight tube by pulsed voltages, V_{ex} and V_{acc}, deliberately chosen to deviate from space-focusing conditions.[18] Ion arrival time is then a sensitive function of the ion's location when the electric field was applied. Consequently, the ion arrival time distribution (TOF mass spectral peak shape) is a map of the initial neutral fragment velocity distribution.

Two useful limiting cases of the pulsed field TOF method differ in the type of mapping. If the fragment recoil velocity is slow enough relative to the accelerated drift velocity, even the fragments recoiling perpendicular to the extraction direction will strike the 1.3-in.-diameter detector.[19] This arrival time distribution is a projection of the three-dimensional velocity distribution along the extraction direction, modified by the appropriate initial-velocity to flight-time transformation. We call this method the one-dimensional velocity projection technique; it is particularly useful

(1) Busch, G. E.; Mahoney, R. T.; Morse, R. I.; Wilson, K. R. *J. Chem. Phys.* **1969**, *51*, 449. Diesen, R. W.; Wahr, J. C.; Adler, S. E. *J. Chem. Phys.* **1969**, *50*, 3635.
(2) Dzvonik, M.; Yang, S.; Bersohn, R. *J. Chem. Phys.* **1974**, *61*, 4408.
(3) Jackson, W. M. *J. Chem. Phys.* **1973**, *59*, 960. Jackson, W. M.; Cody, R. J. *J. Chem. Phys.* **1974**, *61*, 4183.
(4) Baronavski, A. P.; McDonald, J. R. *Chem. Phys. Lett.* **1977**, *45*, 172.
(5) Kinsey, J. L. *J. Chem. Phys.* **1977**, *66*, 2560.
(6) Schmiedl, R.; Dugan, H.; Meier, W.; Welge, K. H. *Z. Phys. A* **1982**, *304*, 137.
(7) Nadler, I.; Mahgerefteh, D.; Reisler, H.; Wittig, C. *J. Chem. Phys.* **1985**, *82*, 3885.
(8) Koplitz, B.; Xu, Z.; Baugh, D.; Buelow, S.; Häusler, D.; Rice, J.; Reisler, H.; Qian, C. X. W.; Noble, M.; Wittig, C. *Faraday Discuss. Chem. Soc.* **1986**, *82*, 125.
(9) Koplitz, B.; Xu, Z.; Wittig, C. *Chem. Phys. Lett.* **1987**, *137*, 505.
(10) Hall, G. E.; Sivakumar, N.; Ogorzalek, R.; Chawla, G.; Haerri, H.-P.; Houston, P. L.; Burak, I.; Hepburn, J. W. *Faraday Discuss. Chem. Soc.* **1986**, *82*, 13.
(11) Chandler, D. W.; Houston, P. L. *J. Chem. Phys.* **1987**, *87*, 1445.
(12) Riley, S. J.; Wilson, K. R. *Discuss. Faraday Soc.* **1972**, *53*, 132.
(13) Sparks, R. K.; Shobatake, K.; Carlson, L. R.; Lee, Y. T. *J. Chem. Phys.* **1981**, *75*, 3838.
(14) Hermann, H. W.; Leone, S. R. *J. Chem. Phys.* **1982**, *76*, 4766.
(15) Van Veen, G. N. A.; Baller, T.; De Vries, A. E.; Van Veen, N. J. A. *Chem. Phys.* **1984**, *87*, 405.
(16) Barry, M. D.; Gorry, P. A. *Mol. Phys.* **1984**, *52*, 461.
(17) Dietz, T. G.; Duncan, M. A.; Liverman, M. G.; Smalley, R. E. *J. Chem. Phys.* **1980**, *73*, 4816.
(18) Wiley, W. C.; McLaren, I. H. *Rev. Sci. Instrum.* **1955**, *26*, 1150.
(19) MM-1 Particle Multiplier, Johnston Laboratories, Cockeysville, MD 21030.

0022-3654/88/2092-0005$01.50/0

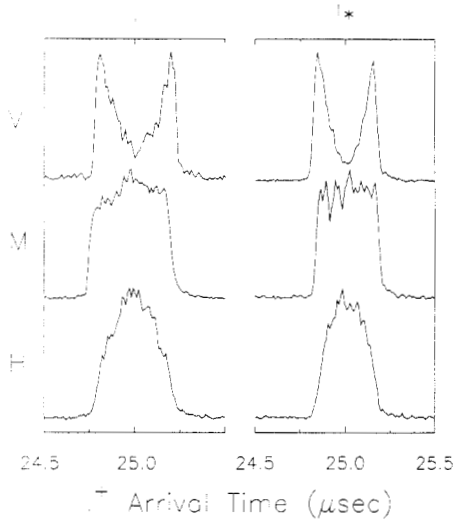

Figure 1. One-dimensional velocity projections for I and I* fragments from the 266-nm dissociation of CH_3I monomers. I and I* were probed at 303.6 and 308.0 nm. Rows labeled V, H, and M correspond to vertical, horizontal, and magic angle 266-nm polarization, with reference to a vertical extraction direction. Each signal is the sum of transient records from 500 laser shots.

for measuring angular distributions of monoenergetic fragments. Alternatively, if the fragment recoil velocity is fast enough, fragments recoiling laterally will miss the detector. In the extreme case, only fragments recoiling up or down along the extraction direction are detected. The arrival time distribution is then a one-dimensional sample through the core of the full three-dimensional velocity distribution. Deflection electrodes at the base of the flight tube allow the ion distribution to be centered on the detector, an essential feature of this method. This one-dimensional sampling technique is particularly useful for determining the correlation between states of different photofragments and for resolving multiple pathways to the same fragment ion that differ in kinetic energy.

Results and Discussion

Angular Distributions of Photofragments and Velocity Projections. Time-of-flight data reflecting the angular distributions of $I(^2P_{3/2})$ and $I^*(^2P_{1/2})$ photofragments from the 266-nm dissociation of CH_3I illustrate the one-dimensional velocity projection technique in Figure 1. I and I* fragments ionized at 308.0 and 303.6 nm[20] are displayed. Essentially identical results were obtained for 266-nm photolysis and several other I and I* 2 + 1 ionization resonances in the 260–315-nm region or for one-laser photolysis/ionization on resonances between 270 and 282 nm. The upper panels were recorded with the 266-nm dissociation laser polarized along the vertical extraction direction of the TOF spectrometer. Prompt dissociation following a parallel absorption results in fragments recoiling preferentially along the polarization axis. The early and late components of the arrival time distribution for I and I* correspond to the upward and downward velocity components of the neutral recoiling fragments for the voltages and delay used here: V_{ex} = 100 V/2.54 cm, V_{acc} = 1900 V/1.27 cm, τ_D = 250 ns. These conditions were chosen to give a nearly linear initial-velocity to flight-time transformation, so the peak shapes look similar to Doppler profiles of photofragments.[5-7]

By rotating the polarization of the 266-nm dissociation laser with a waveplate, we can obtain projections along other directions. The lower panel of Figure 1 shows the arrival time distributions for the polarization perpendicular to the flight tube, and the center panel shows the arrival time distribution for the polarization rotated by the magic angle, 54.7°, from the flight tube. The 25% higher recoil velocity of I compared to I* is evident from the difference in peak widths displayed in Figure 1. The kinetic energy

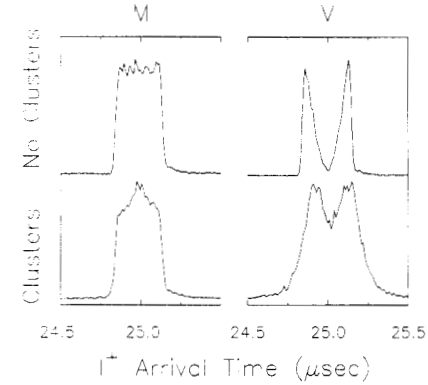

Figure 2. One-dimensional velocity projections for I* fragments from the 266-nm dissociation of CH_3I monomers (upper traces) and clusters (lower traces) for either magic angle or vertical polarization, as labeled.

distributions of the atomic fragments are not completely sharp but have a ±8% variation in the I or I* velocity due to the range of internal energies of sibling methyl fragments.[13] Approximating the I or I* kinetic energies with one average value, we can simulate the arrival time distributions using measured instrumental distances and voltages along with a single adjustable parameter, β, to characterize the angular distribution. We obtain $\beta = 1.8 \pm 0.1$ for I* and $\beta = 1.7 \pm 0.1$ for I at six two-photon I and I* resonances in the 270–275-nm region. Values for 266-nm photolysis are consistent with these but are subject to a larger uncertainty due to the presence of a small one-laser background signal.

Background signals can occur from either the dissociation laser or the probe laser acting alone to form ions. At most of the wavelengths studied in this work, careful minimization of methyl iodide dimers removed most and sometimes all of the one-laser background. In favorable cases, the two-laser ion signal exceeded the sum of one-laser background by more than 20:1.

Even the pulsed field background signals yield valuable mechanistic detail. The probe laser background from 270 to 350 nm displayed distinctive TOF peak shapes and polarization dependences which frequently allowed us to infer or eliminate possible multiphoton ionization and dissociation mechanisms.[21] From changes in the one-laser TOF signals with variable expansion conditions, we have confirmed that the long-puzzling 266-nm I^+ background[22,23] arose from methyl iodide dimers or higher clusters in the molecular beam.[21]

Monomers and Dimers of Methyl Iodide. The role of dimers and clusters of methyl iodide has been much discussed in the context of molecular beam photodissociation studies.[23] Translational energy measurements offer a particularly clear diagnostic for the origins of photofragments. Whereas the velocity distribution of a state-selected photofragment from a monomer parent molecule may be sharp, the same photofragment from a dimer or a cluster parent may have a broad distribution of velocities. Such a distinction was noted in the Doppler spectra of NO fragments from NO dimers and higher clusters.[24]

As expansion conditions were varied, different TOF peak shapes were observed for both I and I* with our one-dimensional velocity projection technique. The upper left-hand trace in Figure 2 shows the square-topped magic angle TOF peak shape associated with the relatively sharp speed distribution of I* from the monomer. For this measurement the nozzle was heated to 80 °C, the sample was 6% methyl iodide in 2.7 bar of He, and the amount of gas allowed through the nozzle was restricted by a short duration

(20) Gedanken, A.; Robin, M. B.; Yafet, Y. *J. Chem. Phys.* **1982**, *76*, 4798.

(21) Ogorzalek Loo, R. R.; Haerri, H.-P.; Hall, G. E.; Houston, P. L., to be published.

(22) Danon, J.; Zacharias, H.; Rottke, H.; Welge, K. C. *J. Chem. Phys.* **1982**, *76*, 2399. Jiang, Y.; Giorgi-Arnazzi, M. R.; Bernstein, R. B. *Chem. Phys.* **1986**, *106*, 171.

(23) Donaldson, D. J.; Vaida, V.; Naaman, R. *J. Chem. Phys.* **1987**, *87*, 2522. Sapers, S.; Vaida, V.; Naaman, R., private communication.

(24) Casassa, M. P.; Stephenson, J. C.; King, D. S. *Faraday Discuss. Chem. Soc.* **1986**, *82*, 251.

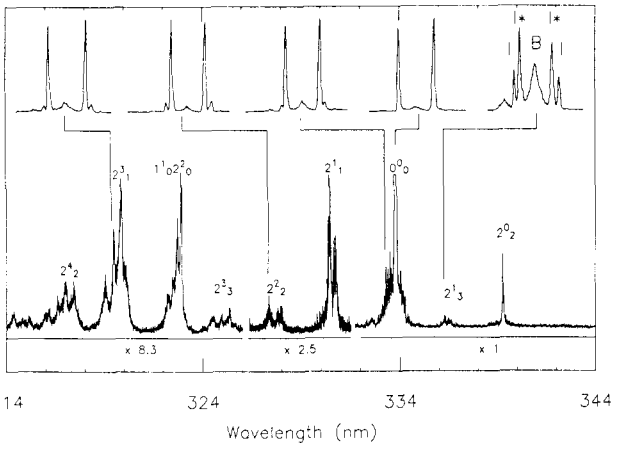

Figure 3. 2 + 1 MPI spectrum of the CD_3 product formed following photodissociation of CD_3I monomers at 266 nm. The labeled vibronic bands all belong to the 3p $^2A_2''$ ← 2p $^2A_2''$ electronic transition. The spectrum is not corrected for variations in dye laser power. One-dimensional samples of the CD_3 recoil distribution were measured at wavelengths indicated by vertical connecting lines. Peaks labeled I and I* correspond to CD_3 from the I and I* channels of the dissociation; the central peak, labeled B, arises from probe laser background CD_3^+.

(<200 μs) open pulse applied to the pulsed valve.[25] When a longer open pulse was applied, moving the beam valve tip farther from the orifice, the TOF peak shape changed to that of the lower left-hand trace. Slower I* fragments appear in the center of the distribution, and faster I* fragments appear in the wings. Similar changes observed with the photolysis laser polarized vertically under unclustered and clustered conditions are illustrated in by the right-hand traces in Figure 2. Even under expansion conditions which generated many dimers, the leading edge of the expansion contained mostly monomers, due to low sample density and/or velocity slip effects, as we judged by the sharpness of the iodine photofragment speed distribution.

The Methyl Fragment from 266-nm Methyl Iodide Dissociation. We have also examined the methyl photofragment in the 266-nm dissociation of CH_3I, as probed using 2 + 1 ionization through the resonant intermediate 3p $^2A_2''$ and 4p $^2A_2''$ Rydberg levels.[26,27] Figure 3 shows an MPI spectrum obtained for CD_3. We concentrated on the 3p $^2A_2''$ 0^0_0, 2^1_1, and 2^2_2 vibronic bands in both CH_3 and CD_3 and the 3p $^2A_2''$ 2^0_2, 2^1_3, 2^3_3, and 2^4_2 in CD_3. The 2^1_3, 2^3_3, and 2^4_2 bands have not been previously observed in either CH_3 or CD_3, while the 2^0_2 band has been reported only for CH_3[28] and the 2^2_2 band only for CD_3.[26] Only umbrella mode excitation (ν_2) has been reported in the methyl fragment from the 266-nm methyl iodide photodissociation.[14]

The one-dimensional sampling limit was approached with V_{ex} = 2000 V/2.54 cm, V_{acc} = 0 V/1.27 cm, and τ_D = 300 ns. This allowed complete resolution of the methyl fragments produced in coincidence with I and I*. The upper insets in Figure 3 show CD_3^+ mass peaks for ν_2 = 0, 1, 2, and 3. The faster methyl radicals arise from the I channel in the dissociation, while the slower ones arise from the I* channel, as labeled in the upper right-hand trace. Probe laser background at this wavelength is responsible for the slowest CD_3 fragments.

We can use this technique to measure I/I* ratios for methyl radicals in individual vibrational levels, or even rotational states, when resolution permits. Ratios of peak areas were corrected for the slight measured differences in β and small differences in ion collection solid angle for methyl fragments arising from the I and I* channels. We further assume that v–J correlations[29] are

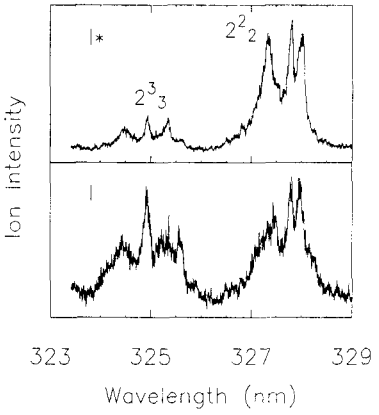

Figure 4. Multiphoton ionization spectra of CD_3 from the 266-nm dissociation of CD_3I recorded near the 2^2_2 and 2^3_3 bands by gating the detection electronics to observe CD_3 radicals produced in coincidence with either I* (upper) or I (lower).

negligible or affect both channels identically. Our results indicate I/I* ratios of <0.05, 0.09, 0.19, and 0.68 for ν_2 = 0–3 CD_3 from the CD_3I dissociation and 0.08, 0.37, and 1.1 for ν_2 = 0–2 CH_3 from CH_3I. Multiple determinations led to estimated uncertainities of about 0.05 in each of these ratios. For each vibronic band we studied, the I/I* ratios increased by factors of 2–4 at wavelengths away from the central peak, where the above ratios were determined. Figure 3 shows examples of data at two wavelengths in the 0^0_0 band with substantially different I/I* ratios. It is interesting that the individual vibronic level I/I* ratios differ for CH_3I and CD_3I, as also observed by Van Veen et al.[15] at 248 nm. While the 266-nm dissociation of CD_3I has not been reported previously, Lee and his group have examined the CH_3I dissociation at this wavelength[13] and report I/I* ratios of 0.03, 0.09, 0.09, and 0.48 for ν_2 = 0–3, respectively. Our results differ markedly from theirs. Recently, Chandler and Houston[11] used a related MPI technique to image ν_2 = 0 methyl radicals. They observed less than 5% methyl radical from the I channel, consistent with our results. Further comparisons for other vibrational states will be possible with forthcoming results from Sandia Laboratories.[30] Our I/I* ratio for ν_2 = 2, combined with the overall I/I* ratio of 0.37,[31] is inconsistent with the previously reported[13] vibrational distribution for photolysis at 266 nm. Our results on the vibrational distribution will be discussed elsewhere.[21]

Finally, we wish to demonstrate a particularly striking and powerful application of this translational imaging technique. By setting boxcar gates on the CD_3^+ mass peaks corresponding to the I and I* channels, we simultaneously obtained separate 2 + 1 MPI spectra for these two channels. The upper and lower panels of Figure 4 display the MPI spectra of CD_3 ν_2 = 2 and 3 measured, respectively, in coincidence with I and I*. There are clear differences in the relative intensities of vibronic bands and their rotational profiles for the two channels. It is expected that the I* is produced in coincidence with low rotational levels, while the I is produced in coincidence with high rotational levels. This trend appears also to occur for ν_2 = 0, as shown in the relevant traces in Figure 3. In this respect, the dissociation of CH_3I would be similar in nature to that of ICN.[32-34] By analogy, we expect that the CH_3 fragment will be rotating primarily about a C_2 axis rather than about the C_3 axis.

Conclusions

The sensitive and versatile new techniques which we have presented here provide the velocity and internal energy information

(25) Adams, T. E.; Rockney, B. H.; Morrison, R. J. S.; Grant, E. R. *Rev. Sci. Instrum.* **1981**, *52*, 1469.
(26) Hudgens, J. W.; Di Giuseppe, T. G.; Lin, M. C. *J. Chem. Phys.* **1983**, *79*, 571.
(27) Chen, P.; Colson, S. D.; Chupka, W. A.; Berson, J. A. *J. Phys. Chem.* **1986**, *90*, 2319.
(28) Smyth, K. C.; Taylor, P. H. *Chem. Phys. Lett.* **1985**, *122*, 518.
(29) Houston, P. L. *J. Phys. Chem.* **1987**, *91*, 5388.
(30) Chandler, D. W.; Parker, D., private communication.
(31) Hess, W. P.; Kohler, S. J.; Haugen, H. K.; Leone, S. R. *J. Chem. Phys.* **1986**, *84*, 2143.
(32) Hall, G.; Sivakumar, N.; Houston, P. *J. Chem. Phys.* **1986**, *84*, 2120.
(33) Nadler, I.; Reisler, H.; Wittig, C. *Chem. Phys. Lett.* **1984**, *103*, 451.
(34) Goldfield, E. M.; Houston, P. L.; Ezra, G. S. *J. Chem. Phys.* **1986**, *84*, 3120.

that is the cornerstone of photodissociation studies. They also provide an excellent window on cluster detection and multiphoton ionization and dissociation pathways. These fast, simple, and inexpensive techniques can be profitably applied in any TOF mass spectrometer.

Acknowledgment. H.-P. Haerri thanks the Swiss National Science Foundation for support during his postgraduate studies. The support of the NSF under Grant CHE-8617062 is gratefully acknowledged. We have benefited from discussions with Steve Penn, Fleming Crim,[35] and David W. Chandler.[30]

(35) Penn, S. M.; Hayden, C. C.; Carlson, K. C.; Crim, F. F. *J. Chem. Phys.*, in press.

Nature of the Bonding and Valence for the Oxygen and Copper in High-Temperature Superconductors

Donald T. Sawyer

Department of Chemistry, Texas A&M University, College Station, Texas 77843 *(Received: October 20, 1987)*

The ionization potentials, electron affinities, and electronegativities for the atoms in the $Ba_2YCu_3O_7$ high-temperature superconductor dictate that electron transfer from Ba and Y to the O atoms will occur to form Y^{3+}, two Ba^{2+}, and seven $O^{\bullet-}$ ions. The latter (s^2p^5 valence shell) form covalent bonds with the three Cu^0 atoms ($d^{10}s$ valence shell) to give one Cu^0–O^- ion ($d^{10}s$–p^5s^2) and two $Cu^0(-O^-)_3^{3-}$ ions [$d^9sp{\equiv}(p^5s^2)_3$]. Electrostatic and lattice forces control the interactions between the $[2Ba^{2+}, Y^{3+}]^{7+}$ and $[Cu^0$–$O^-, 2Cu^0(-O^-)_3^{3-}]^{7-}$ ions to give the orthorhombic structure of the $Ba_2YCu_3O_7$ superconductor.

The intense characterization efforts directed to the newly discovered high-temperature superconductors[1-3] have established that they are a different class of materials from classical metallic superconductors.[4] Although the debate is vigorous as to the mechanism of superconduction for the rare earth copper oxides,[5-8] there is agreement that it must be different from that for metal alloys and accommodate chemical interaction (bonding) between the copper and oxygen atoms.[7] The materials have the physical appearance, composition, and mechanical properties of ceramics.[9,10]

The most completely characterized material, $Ba_2YCu_3O_7$, has an orthorhombic structure with two sets of copper atoms and four sets of oxygen atoms.[1] For a ceramic-like material the interactions of the component atoms will be dominated by covalent and ionic bonding via their valence electrons. The nonbonding electrostatic and lattice forces will be secondary, but critical to the structural arrangement of the ionic groups.

The electron distribution and nature of the bonding among the atoms of $Ba_2YCu_3O_7$ are controlled by their ionization potentials, electron affinities, and electronegativities. Table I summarizes these parameters for the elements of $Ba_2YCu_3O_7$, as well as the redox thermodynamics for copper and oxygen in an inert solvent matrix and the gas-phase bond energies for copper–oxygen molecules.[11-17]

TABLE I: Electronic Character of Elements of $Ba_2YCu_3O_7$

A. Gas-Phase Electronic Energies

	ionizn potential,[a] eV	electronic affinity,[b] eV	electronegativity χ (Mulliken)[c]	electronegativity χ (Pauling)[d]
Ba	5.21, 10.0	~0.0	0.83	0.89
Y	6.38, 12.2, 20.5	0.31	1.06	1.22
Cu	7.73, 20.3, 36.8	1.24	1.42	1.90
O	13.62, 35.1	1.46	2.39	3.44

B. Reduction Potentials in Acetonitrile[e]

	$E°'$, V vs NHE
$Cu^{3+} + e^- \rightarrow Cu^{2+}$	+2.7 (est)
$Cu^{2+} + e^- \rightarrow Cu^+$	+1.29
$Cu^+ + e^- \rightarrow Cu^0$	−0.09
$O(g) + e^- \rightarrow O^{\bullet-}$	+0.67
$O^{\bullet-} + H_2O + e^- \rightarrow 2^-OH$	+0.59
$O^{\bullet-} + e^- \rightarrow O^{2-}$	−3.0 (est)

C. Gas-Phase Bond Energies[f]

	BE, kcal mol^{-1}
Cu–Cu	46.6
O=O	119.1
O–O	~80 (est)
Cu–O	64.3
Cu–O^-	73 (est)

[a] Reference 11. [b] Reference 12. [c] χ (Mulliken) = [(ionization potential) + (electron affinity)]/6.30; ref 13. [d] Reference 14. [e] Reference 15 and 16. [f] Reference 17.

Contemporary analyses of the atomic interactions in copper–oxygen superconductors have assumed that the oxygen atoms carry eight valence electrons with the chemical character of oxo dianions.[5,7,8] For $Ba_2YCu_3O_7$ this amounts to a total negative charge of $14e^-$, which must be balanced with seven positive charges from three copper ions (two Cu^{2+} and one Cu^{3+}) in addition to seven positive charges from two Ba^{2+} and one Y^{3+} ions. The redox

(1) Beech, F.; Miraglia, S.; Santoro, A.; Roth, R. S. *Phys. Rev. B* **1987**, *35*, 8778.
(2) Cava, R. J.; Batlogg, B.; Van Dover, R. B.; Murphy, D. W.; Sunshine, S.; Siegrist, T.; Remeika, J. P.; Rietman, E. A.; Zahurak, S.; Espinosa, G. P. *Phys. Rev. Lett.* **1987**, *58*, 1676.
(3) LePage, Y.; McKinnon, W. R.; Tarascon, J. M.; Green, L. H.; Hull, G. W.; Hwang, D. M. *Phys. Rev. B* **1987**, *35*, 7245.
(4) Beasley, M. R.; Geballe, T. H. *Phys. Today* **1984**, *36*, 60.
(5) Anderson, P. W.; Baskaran, G.; Zou, Z.; Hsu, T. *Phys. Rev. Lett.* **1987**, *58*, 2790.
(6) Kivelson, S. A.; Rokhsar, D. S.; Sethna, J. P. *Phys. Rev. B* **1987**, *35*, 8865.
(7) Emery, V. J. *Phys. Rev. Lett.* **1987**, *58*, 2794.
(8) Pauling, L. *Phys. Rev. Lett.* **1987**, *59*, 225.
(9) Wang, H. H.; Carlson, K. D.; Geiser, U.; Thorn, R. J.; Kao, H.-C. I.; Beno, M. A.; Monaghan, M. R.; Allen, T. J.; Proksch, R. B.; Stupka, D. L.; Williams, J. M.; Flandermeyer, B. V.; Poeppel, R. B. *Inorg. Chem.* **1987**, *26*, 1476.
(10) Wu, M. K.; Ashburn, J. R.; Torng, C. J.; Hor, P. H.; Meng, R. L.; Gao, L.; Huang, Z. J.; Wang, Y. Q.; Chu, C. W. *Phys. Rev. Lett.* **1987**, *58*, 908.
(11) *CRC Handbook of Chemistry and Physics*, 68th ed.; CRC: Boca Raton, FL, 1987; pp E-76, E-77.
(12) *CRC Handbook of Chemistry and Physics*, 68th ed.; CRC: Boca Raton, FL, 1987; p E-63.
(13) Pritchard, H. O.; Skinner, H. A. *Chem. Rev.* **1955**, *55*, 745.
(14) Allred, A. L. *J. Inorg. Nucl. Chem.* **1961**, *17*, 215.
(15) Sawyer, D. T.; Roberts, J. L., Jr.; Tsuchiya, T.; Srivatsa, G. S. In *Oxygen Radicals in Chemistry and Biology*; Bors, W., Saran, M., Tait, D., Eds.; Walter de Gruyter: New York, 1984; pp 25–34.
(16) Tsang, P. K. S.; Cofrē, P.; Sawyer, D. T. *Inorg. Chem.* **1987**, *26*, 3604.
(17) Derr, J. A. In *Handbook of Chemistry and Physics*, 68th ed.; CRC: Boca Raton, FL, 1987; pp F-168–F-177.

0022-3654/88/2092-0008$01.50/0